Phys. Status Solidi B **254,** No. 8, 1600668 (2017) / **DOI** 10.1002/pssb.201600668

physica status solidi b
www.pss-b.com
basic solid state physics

Origin of high hole concentrations in Mg-doped GaN films

A. M. Fischer*[,1], S. Wang[1], F. A. Ponce[1], B. P. Gunning[2], C. A. M. Fabien[2], and W. A. Doolittle[2]

[1] Department of Physics, Arizona State University, Tempe, AZ 85287-1504, USA
[2] Advanced Semiconductor Technology Facility, School of Electrical and Computer Engineering, Georgia Institute of Technology, Atlanta, GA 30332, USA

Received 10 October 2016, revised 23 February 2017, accepted 27 March 2017
Published online 19 April 2017

Keywords cathodoluminescence, charge carrier concentration, holes, metal-modulated epitaxy, nitrogen, vacancies

* Corresponding author: e-mail alec.fischer@asu.edu, Phone: +1 480 727 6309, Fax: +1 480 965 2747

The origin for high hole concentration in Mg-doped GaN films grown by metal-modulated epitaxy has been explored. We observe a Mg acceptor band characterized by a broad emission without phonon replicas and a high energy tail that overlaps with the valence band of GaN, giving rise to a reduced effective Mg activation energy. We attribute the high hole concentrations to the reduction of compensating nitrogen vacancy concentration and to effectively dispersed Mg atoms, which are incorporated into the lattice as single substitutional atoms. This has been achieved by a low temperature growth, a decrease in the III/V ratio, and a planar growth interface that results from the layer-by-layer approach using the metal-modulated epitaxial technique.

1 Introduction Substitutional magnesium in a gallium site (Mg_{Ga}) is the preferred acceptor for *p*-type doping in GaN due to its low activation energy, with reported values between 155 and 230 meV [1–4]. The uncertainty in the value has been related to the formation of an acceptor band, with a broad optical emission peaking at ~3.2 eV [3, 5–7]. The nature of this emission has been assigned to a native donor–acceptor pair (DAP_{native}) recombination characterized by a non-exponential radiative decay [8]. The origin of the donor and acceptor centers is rather controversial; with candidates for donors including nitrogen vacancies (V_N), substitutional oxygen in nitrogen sites (O_N), and substitutional silicon in gallium sites (Si_{Ga}) [9–12]. Candidates for acceptors are substitutional Mg and C, as well as gallium vacancies (V_{Ga}) [1, 2, 13, 14].

The realization of high hole concentrations in *p*-type GaN films is currently one of the limiting factors for obtaining highly efficient GaN-based optoelectronic devices. One reason for the low hole concentration in Mg-doped GaN films has been assigned to the presence of hydrogen. The metalorganic vapor chemical deposition (MOVCD) technique typically utilizes ammonia (NH_3) during Mg-doped GaN film growth. The high concentration of hydrogen from ammonia dissociation at high temperatures is thought to passivate Mg by forming electrically inactive Mg-H complexes [15], thus reducing the hole concentration due to a decrease in the effective number of Mg atoms acting as acceptors. Low-energy electron-beam irradiation (LEEBI) and thermal annealing improved *p*-type conductivity [6, 16], possibly by dissociation of Mg-H complexes. These post-growth treatments are not necessary when growing Mg-doped GaN by molecular beam epitaxy (MBE) due to the absence of hydrogen [17, 18]. Low hole concentration is also attributed to self-compensation in heavily Mg-doped GaN films by the association of a Mg_{Ga} acceptor with a V_N donor; the latter is believed to be abundant due to its low formation energy in *p*-type GaN [19]. Heavily Mg-doped GaN-based films have also been found to form Mg precipitates that prevent acceptor state formation [20–23].

Improved *p*-type doping has been reported by growing under N-rich conditions at low temperatures [24–26], which enhances Mg incorporation [24] and reduces the V_N concentration [27]. However, growth under N-rich conditions has a tendency toward formation of crystal facets, surface roughening, and generation of crystal defects [28]. Growth under Ga-rich conditions has the opposite effect. Modulating the growth scheme from a Ga- to N-rich conditions, using the metal-modulated epitaxy (MME) technique in the MBE chamber, has shown to optimize Mg incorporation and crystalline quality [29, 30].

In this letter, we report on the origin of high hole concentration in GaN films. We observe that GaN films grown by MME and doped with Mg at concentra tions above the estimated solid solubility limit of $\sim 1 \times 10^{20}\,\mathrm{cm}^{-3}$ [31], do not present Mg precipitates in their microstructure and exhibit a reduction of the native point defect concentration with increasing Mg concentrations. This is evidenced by: (i) the quenching of longitudinal-optical (LO) phonon replicas; (ii) the $\mathrm{DAP_{native}}$ energy peak red shift; and (iii) the saturation of the $\mathrm{DAP_{native}}$ emission intensity at high carrier injection currents. In addition, as the Mg concentration is increased, the Mg acceptor forms an acceptor band that eventually intercepts the valence band, giving rise to the absence of carrier freeze-out, and resulting in high hole concentrations even at low temperatures [30].

2 Growth Mg-doped GaN epitaxial layers were grown at 600 °C by MME with a thickness in the range of 180–330 nm on a 100-nm thick unintentionally doped AlN layer on c-sapphire substrates. The chamber pressure during growth was $\sim 10^{-5}$ Torr, with a 1.3 sccm of N_2 flow at 350 W of RF power, and with a net growth rate of $\sim 350\,\mathrm{nm\,h}^{-1}$. The modulation cycle was 5 s open/10 s closed, and the Ga and Mg cells were shuttered simultaneously [30, 32]. In order to obtain a range of Mg concentrations, the Mg cracker temperature was varied from 280 to 305 °C, and the III/V ratio from 1.17 to 1.6. No post-growth thermal annealing was necessary to achieve high hole concentrations [17, 18]. The Mg concentration in the GaN film was profiled by secondary ion mass spectroscopy (SIMS) on a Cameca IMS-6f instrument; using O^{2+} ions with a beam current of 100 nA and a raster size of 250 μm.

3 Magnesium activation energy The room temperature hole concentration, mobility, and resistivity of the Mg-doped GaN films were determined by Hall effect measurements following the van der Pauw method [30], using a 0.3 T fixed magnet. The samples were 1×1 cm squares, and the contacts were soldered indium dots. Due to the very high Mg concentrations in these films, the quality of the ohmic contacts were verified via *I–V* sweeps on all contact pairs. The Hall scattering factor used herein was assumed to be 1.

GaN with the wurtzite crystal structure exhibits polarization effects that can affect the electric conductivity of the material. In our case, we are dealing with $+c$-oriented *p*-GaN on AlN, where the only possible polarization-related effect will occur at the *p*-GaN/AlN interface in the form a two-dimensional hole gas (2DHG), as discussed in greater detail by Gunning et al. [32] In our case, Hall effect measures the net sheet charge density σ_{Hall} in the *p*-GaN film, which is the sum of the bulk sheet charge density σ_{bulk} and the 2DHG sheet charge density σ_{2DHG} at the *p*-GaN/AlN interface. The bulk hole concentration $[\mathrm{h}^+]$, shown in Table 1, is then calculated by the following equation:

$$[\mathrm{h}^+] = \frac{\sigma_{\mathrm{bulk}}}{d} = \frac{(\sigma_{\mathrm{Hall}} - \sigma_{\mathrm{2DHG}})}{d} \tag{1}$$

where d is the *p*-GaN thickness. The magnitude of σ_{2DHG} is 3.25×10^{13} for a fully relaxed *p*-GaN film and $5.3 \times 10^{13}\,\mathrm{cm}^{-2}$ for a fully strained one [32]. We believe that the *p*-GaN film is close to a fully relaxed case since its thickness is much larger than the critical thickness of ~3 nm for misfit strain relaxation on AlN [32]. The results thus obtained are listed in Table 1.

The effective Mg activation energy E_A for a single acceptor level is calculated using the charge neutrality equation:

$$p - N_A^- = n - N_D^+ \tag{2}$$

which is equivalent to:

$$\frac{2}{\sqrt{\pi}} N_V F_{1/2}\left(\frac{E_V - E_F}{k_B T}\right) - \frac{N_A}{1 + g_A e^{\frac{(E_A - E_F)}{k_B T}}} = \frac{2}{\sqrt{\pi}} N_C F_{1/2}\left(\frac{E_F - E_C}{k_B T}\right) - \frac{N_D}{1 + g_D e^{\frac{(E_F - E_D)}{k_B T}}} \tag{3}$$

where k_B is the Boltzmann constant, T is the temperature, N_C and N_V are the effective density of states in the conduction and valence band. The effective masses used for the density of states are 0.2 for electrons and 0.8 for holes. $g_A = 4$ and $g_D = 2$ are the degeneracy factors for acceptors and donors.

Table 1 Electrical properties of Mg-doped GaN obtained from Hall measurements. The magnesium concentration [Mg] was measured by SIMS. The film hole concentration $[\mathrm{h}^+]$ is obtained by subtracting the 2DHG from the Hall effect hole concentration.

sample	[Mg] ($\times$lO^{20} cm^{-3})	$[\mathrm{h}^+]$ ($\times$lO^{19} cm^{-3})	doping efficiency (%)	mobility ($\mathrm{cm^2\,V^{-1}\,s^{-1}}$)	conductivity $(\Omega\,\mathrm{cm})^{-1}$	effective Mg activation energy (meV)
A	0.58	0.286	5	1.96	0.90	90
B	1.20	0.825	7	1.10	1.41	50
C	1.50	2.76	18	0.55	2.44	0
D	2.64	4.45	17	0.34	2.44	0

E_F is the Fermi energy level, E_A is the effective acceptor activation energy and $E_D = 0.03$ eV is the effective donor activation energy.

E_C and E_V are the energies of the bottom of the conduction and the top of the valence band. The background donor concentration N_D is assumed to be 10^{17} cm^{-3}. $F_{1/2}$ is the Fermi-Dirac integral and was calculated using a short series approximation [33]. The numerical solution expresses a reasonable value of E_A irrespective of whether E_F is above or below $3k_BT$ with respect to the valence band. The calculated effective Mg activation energy decreases from 90 (sample *A*) to 0 meV (samples *C* and *D*), suggesting that for sufficiently high Mg concentrations the Mg acceptor level intercepts the valence band, rendering the GaN degenerate [32]. This agrees with the high hole concentrations ($[h^+] \gg 10^{18}$ cm^{-3}) and the absence of carrier freeze-out previously observed at low temperatures [28]. Although this calculation is for a single acceptor level E_A and not for an acceptor band, there is a clear trend for the decrease of the effective Mg activation energy with increasing Mg concentration.

In Table 1, we notice that the doping efficiency, defined as $[h^+]/[Mg]$, increases with doping concentration. Sample *D* has the highest Mg concentration of 2.64×10^{20} cm^{-3} that corresponds to a doping efficiency of ~17% [17, 34]. The measured Mg concentration is higher than the estimated solid solubility limit in GaN. Magnesium solubility in GaN is the determining factor limiting the hole concentration [19]. Mg concentrations at and/or near the solubility limit in GaN have been shown by TEM to be associated with the formation of Mg-related inversion domains and precipitates with lateral dimensions of the order of 50 nm [20–23]. No such precipitates were observed by TEM in any of our films as shown in Fig. 1.

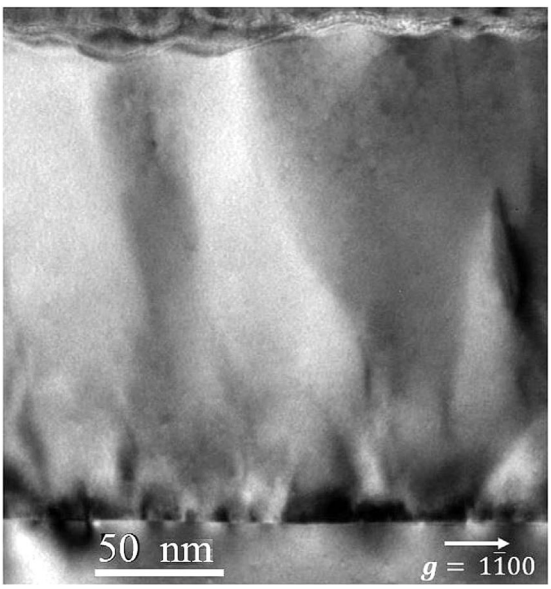

Figure 1 Two-beam bright-field cross-section TEM image of the p-GaN film with the highest Mg concentration. The p-GaN film does not exhibit Mg precipitates.

4 Results and discussion The optical properties associated with Mg doping were studied using cathodoluminescence (CL) spectroscopy in a scanning electron microscope, with a spectrometer equipped with a 1200 l/mm grating and a GaAs photomultiplier tube. The CL spectra were taken at 4.5 and 295 K, with an electron beam current of 400 pA, an acceleration voltage of 5 kV, and a raster size of 34 μm. No further Mg activation was observed resulting from LEEBI effects, as verified by comparing CL and photoluminescence spectra (not shown here). A broad emission band ranging from 2.9 to 3.5 eV, with an energy peak maximum at ~3.25 eV, is observed in all four samples. Figure 2 shows CL spectra taken at 4.5 K of GaN films with the lowest and highest Mg concentrations. Each spectrum can be fitted by two main Gaussian peaks. The first one is labelled DAP_{native} centered at ~3.25 eV, and has two LO-phonon replicas separated by ~92 meV. This DAP transition is usually observed in Mg-doped GaN films, where the donor and acceptor have been assigned to native point defects [2, 35], and it is not associated with *p*-type conductivity [3]. The second one is a broad peak centered at ~3.15 eV, labelled here as DAP_{Mg}, which has been shown to depend on Mg concentration [35]. DAP emission energy $h\nu_{DAP}$ can be expressed by the following equation [36]:

$$h\nu_{DAP} = E_g - E_D - E_A + E_C \quad (4)$$

where E_g is the GaN bandgap, E_D and E_A are the donor and acceptor activation energies, and E_C is the Coulomb energy defined as $e^2/(4\pi\varepsilon(0) \cdot r_{DA})$ with the electron charge ε, and the static dielectric constant $\varepsilon(0)$. The value r_{DA} is defined as distance between donor and acceptor sites and it is inversely

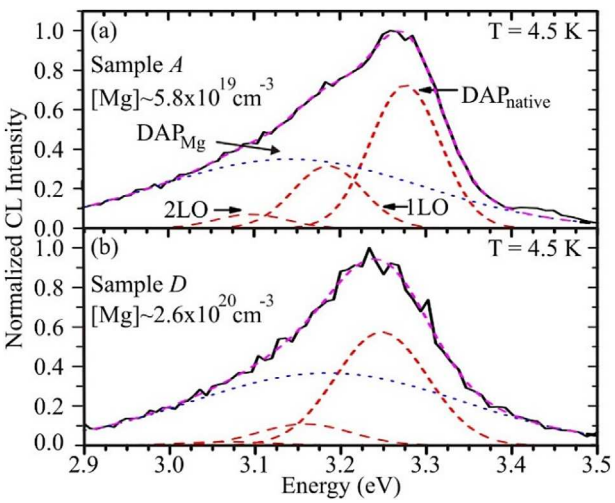

Figure 2 Normalized CL spectra taken at 4.5 K for samples with (a) the lowest and (b) the highest Mg concentration. Best-fit Gaussian curves represent DAP_{native} emission with two LO-phonon replicas (red dash line) and Mg-related DAP (DAP_{Mg}) emission (blue dot line).

proportional to the cube root of the donor (acceptor) concentration N. The recombination of an electron with a hole leads to the emission of phonons caused by the electron (hole)–phonon interaction. In case of strong phonon-coupling, that is strong interaction with the lattice, several replicas can be observed. The appearance of phonon replicas in the DAP_{native} emission suggests that the donor/native occupy lattice sites with strong phonon-coupling. On the other hand, the DAP_{Mg} transition does not exhibit phonon replicas, suggesting weaker coupling and perhaps suggesting that Mg forms an acceptor band. A red shift in DAP_{native} and a blue shift in DAP_{Mg} peak positions with increasing Mg concentration are observed in Fig. 2. The DAP emission red and blue shift are related to the reduction in the native impurity concentration and to the increase in the Mg concentration, respectively, which results from changes in the Coulomb energy of the DAP transition as expressed in Eq. (4). The decrease in the phonon replica intensities in the highest Mg concentration film as shown in Fig. 2(b), indicates a weaker phonon coupling between the native impurities and the lattice, possibly due to a reduction of the native impurity concentration by the lowered III/V ratio, which favors the reduction of V_N formation.

Figure 3 shows CL spectra of samples A and D, taken at room temperature where the phonon replicas are suppressed by thermal effects. Therefore, two Gaussian curves, one each for DAP_{native} and DAP_{Mg}, are sufficient to fit the DAP region at sufficiently high temperatures. The high energy tail of the DAP_{Mg} emission crosses the vertical dashed line which represents the 3.43 eV band gap of GaN at room temperature. This can be interpreted as the Mg acceptor level intercepting the valence band. This idea agrees with the reduced effective Mg activation energy calculated in Table 1.

To determine the effects of Mg concentration on the luminescence properties, we plot in Fig. 4 the energy peak

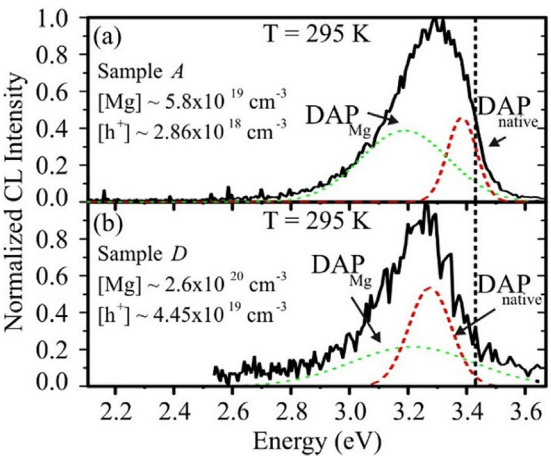

Figure 3 CL spectra for samples A and D taken at 295 K. Red and green dashed Gaussian curves represent DAP_{native} and the DAP_{Mg} emissions, respectively. Increasing Mg concentration results in a red shift of DAP_{native} and a blue shift of the DAP_{Mg}.

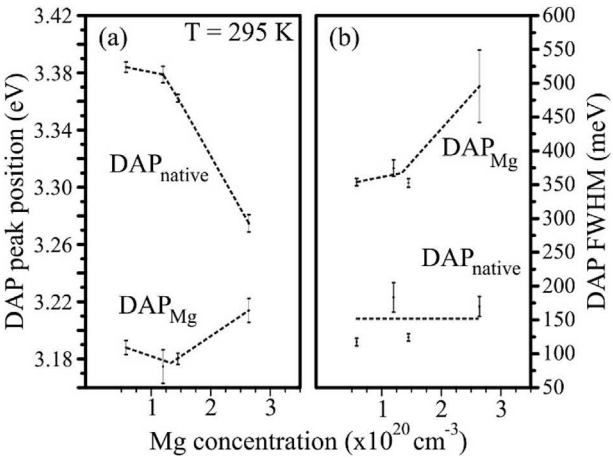

Figure 4 Dependence of the DAP (a) peak position and (b) full-width-at-half-maximum (FWHM) as a function of Mg concentration at 295 K. In (a), the DAP_{native} redshifts with increasing [Mg], whereas the DAP_{Mg} blueshifts. In (b), the DAP_{native} FWHM does not vary with increasing [Mg], suggesting DAP_{native} is not related to Mg.

position and full-width-at-half-maximum (FWHM) of both DAP emission peaks, extracted from CL spectra like in Fig. 3, as a function of Mg concentration. In Fig. 4(a), the DAP_{native} peak emission exhibits a red shift of up to 100 meV with increasing Mg concentration, whereas the DAP_{Mg} shows a blue shift of ~20 meV. A DAP red shift can be associated to a reduction in the Coulomb interaction which is inversely proportional to the spatial separation of ionized donors and acceptors. The observed DAP_{native} red shift is due to a reduction of the Coulomb interaction as their relative concentrations decrease as a result of increasing Mg concentration [36]. In a similar manner, the increase in Mg concentration in Fig. 4(a) leads to the blue shift of the DAP_{Mg}.

The FWHM of the DAP_{native} emission in Fig. 4(b) remains fairly constant with increasing Mg concentration, confirming that its optical transition does not involve a Mg acceptor. On the other hand, the FWHM of the DAP_{Mg} emission exhibits an increase of ~150 meV with Mg concentration, indicating the widening of the acceptor band toward the valence band edge. Figure 5 compares CL spectra of p-type GaN films grown by MME and MOCVD with [Mg] in the range of $2–5 \times 10^{19}\,cm^{-3}$ [37]. The sharp emission at 3.471 eV of the MOCVD-grown film is associated to the underlying unintentionally-doped GaN film. The high energy tail of the DAP region in the MME-grown film crosses the GaN valence band at ~3.5 eV, which is not the case in the MOCVD case. The MOCVD-grown p-type GaN exhibits a DAP region at lower energies, suggesting a lower chance of the DAP_{Mg} intercepting the valence band. This could exlpain why high hole concentrations and absence of carrier freeze-out have only been observed in films grown by MME [30].

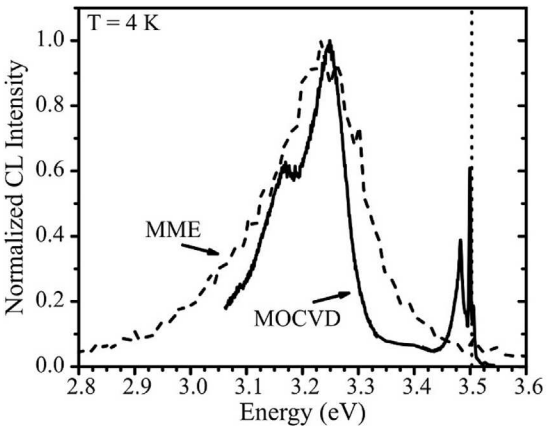

Figure 5 Low-temperature CL spectra of *p*-type GaN grown by MOCVD (solid line) [37] and MME (dashed line), with [Mg] in the $2–5 \times 10^{19}\,cm^{-3}$ range.

The reduction of the native impurity concentration with increasing Mg concentration, as suggested in Figs. 2(b) and 4(a), can be further observed by comparing the total DAP emission for various Mg concentrations as a function of carrier injection density, as shown in Fig. 6. The carrier injection is generated in the solid by the electron beam in the SEM. The black solid line and the red dashed line spectra were taken under low and high carrier injection densities, $J_{low} = 4 \times 10^{13}$ and $J_{high} = 10^4 x J_o = 4 \times 10^{17}$ e–h pairs cm^{-3}, respectively. As mentioned for Fig. 3, the DAP region consists of two luminescence peaks, DAP_{native} and DAP_{Mg}. At low Mg concentrations in Fig. 6(a), the increase in carrier injection density does not alter the shape of the DAP region. This means that the donor and acceptor concentrations of both DAP recombination channels are sufficiently large and do not saturate at higher injection densities. At intermediate Mg concentrations, in Fig. 6(b) and (c), we observe a progressive red shift of the DAP peak at higher carrier injection densities. The DAP region maintains an asymmetric shape suggesting that the contribution of both DAPs is still present at high injection densities, with a slight contribution of the DAP_{Mg} transition. However, this is not the case for sample *D* with the highest Mg concentration seen in Fig. 6(d), where the DAP region is symmetric at high carrier injection densities. This indicates that the DAP_{Mg} recombination channel is now dominant and the DAP_{native} transition has saturated. Sample *D* was grown at lower III/V ratios and higher Mg cracker temperatures. One way to interpret our observations is to consider the growth parameters: (i) Increasing the Mg cracker temperature naturally is expected to increase the [Mg]. (ii) Decreasing the III/V ratio is expected to: (a) increase the density of group-III sites, facilitating the incorporation of Mg in Ga sites as substitutional acceptors; and (b) decrease the nitrogen vacancy (V_N) (i.e., native impurity) concentration, reducing the known compensating effect on Mg acceptors in *p*-type GaN. A decrease in V_N concentration is responsible for the saturation of the DAP_{native} transition at high injection densities, because $J_{high} > [V_N]$ at high Mg concentrations. The observed quenching of the DAP_{native} LO-phonon replicas from Fig. 2(a) to (b), and the observed red shift of the DAP_{native} with increasing Mg concentration, in Fig. 4(a), further support the idea of the decrease of this native impurity concentration as discussed earlier.

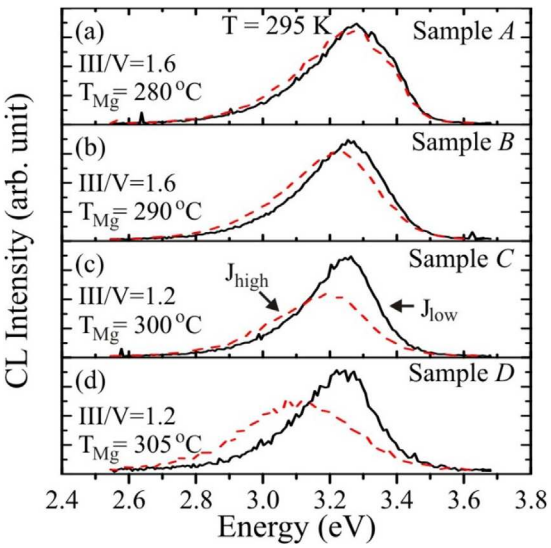

Figure 6 Effect of carrier injection density on the DAP emission. Black solid line CL spectra were taken at low carrier injection densities J_{low} while the red dashed line CL spectra were taken at J_{high}. The DAP emission exhibits an increasing red shift from (a) to (d) as the [Mg] increases due to saturation of the DAP_{native} recombination channel.

5 Conclusions We have studied the optical, electrical, and structural properties of Mg-doped GaN. We report that the absence of LO-phonon replicas in the DAP_{Mg} emission and an increase of its FWHM with increasing Mg concentration confirm the existence of a Mg acceptor band, which is found to intercept the valence band of GaN, resulting in the increase of the hole concentration and in the elimination of carrier freeze-out, as has already been observed in similar materials grown by the MME technique. The observations consist of (i) quenching of the DAP_{native} LO-phonon replicas, (ii) red shift of the DAP_{native} emission energy, and (iii) saturation of the DAP_{native} emission intensity at high carrier injection current densities. Our studies show that the native impurity concentration V_N decreases with increasing Mg concentration, and support the notion that higher Mg cracker temperature and the decrease in the III/V ratio facilitates the incorporation of Mg as substitutional acceptors. No precipitates were found, even for Mg concentrations higher than the estimated solid solubility limit, indicating that metal-modulated epitaxy with proper growth conditions optimizes lateral diffusivity of Mg as well as Mg incorporation, while maintaining a layer-by-layer growth.

Acknowledgements This study was supported in part by the National Science Foundation (NSF) and the Department of Energy (DOE) under NSF CA No. EEC-1041895, by the NSF Materials World Network under grant NSF CA No. DMR -1108450, and by the Advanced Research Projects Agency-Energy (ARPA-E), U.S. Department of Energy, Focus Program under grant DE-AR0000470.

References

[1] I. Akasaki, H. Amano, M. Kito, and K. Hiramatsu, J. Lumin. **48–49**, 666 (1991).
[2] S. Fischer, C. Wetzel, E. E. Haller, and B. K. Meyer, Appl. Phys. Lett. **67**, 1298 (1995).
[3] W. Götz, N. M. Johnson, J. Walker, D. P. Bour, and R. A. Street, Appl. Phys. Lett. **68**, 667 (1996).
[4] W. Kim, A. Salvador, A. E. Botchkarev, O. Aktas, S. N. Mohammad, and H. Morcoç, Appl. Phys. Lett. **69**, 559 (1996).
[5] H. P. Maruska, D. A. Stevenson, and J. I. Pankove, Appl. Phys. Lett. **22**, 303 (1973).
[6] H. Amano, M. Kito, K. Hiramatsu, and I. Akasaki, Jpn. J. Appl. Phys. **28**, L2112 (1989).
[7] U. Kaufmann, M. Kunzer, M. Maier, H. Obloh, A. Ramakrishnan, B. Santic, and P. Schlotter, Appl. Phys. Lett. **72**, 1326 (1998).
[8] R. Dingle and M. Ilegems, Solid State Commun. **9**, 175 (1971).
[9] H. P. Maruska and J. J. Tietjen, Appl. Phys. Lett. **15**, 327 (1969).
[10] B. C. Chung and M. Gershenzon, J. Appl. Phys. **72**, 651 (1992).
[11] P. Perlin, T. Suski, H. Teisseyre, M. Leszczynski, I. Grzegory, J. Jun, S. Porowski, P. Boguslawski, J. Bernholc, J. C. Chervin, A. Polian, and T. D. Moustakas, Phys. Rev. Lett. **75**, 296 (1995).
[12] S. Nakamura, T. Mukai, and M. Senoh, Jpn. J. Appl. Phys. **31**, 2883 (1992).
[13] J. Neugebauer and C. G. Van de Walle, Appl. Phys. Lett. **69**, 503 (1996).
[14] K. Saarinen, T. Laine, S. Kuisma, J. Nissilä, P. Hautojärvi, L. Dobrzynski, J. M. Baranowski, K. Pakula, R. Stepniewski, M. Wojdak, A. Wysmolek, T. Suski, M. Leszczynski, I. Grzegory, and S. Porowski, Phys. Rev. Lett. **79**, 3030 (1997).
[15] S. Nakamura, N. Iwasa, M. Senoh, and T. Mukai, Jpn. J. Appl. Phys. **31**, 1258 (1992).
[16] S. Nakamura, T. Mukai, M. Senoh, and N. Iwasa, Jpn. J. Appl. Phys. **31**, L139 (1991).
[17] M. S. Brandt, N. M. Johnson, R. J. Molnar, R. Singh, and T. D. Moustakas, Appl. Phys. Lett. **64**, 2264 (1994).
[18] J. M. Myoung, K. H. Shim, C. Kim, O. Gluschenkov, K. Kim, S. Kim, D. A. Turnbull, and S. G. Bishop, Appl. Phys. Lett. **69**, 2722 (1996).
[19] C. G. Van de Walle, C. Stampfl, and J. Neugebauer, J. Cryst. Growth **189–190**, 505 (1998).
[20] Z. Liliental-Weber, M. Benamara, J. Washburn, I. Grzegory, and S. Porowski, Phys. Rev. Lett. **83**, 2370 (1999).
[21] Z. Liliental-Weber, M. Benamara, W. Swider, J. Washburn, I. Grzegory, S. Porowski, D. J. H. Lambert, C. J. Eiting, and R. D. Dupuis, Appl. Phys. Lett. **75**, 4159 (1999).
[22] L. T. Romano, J. E. Northrup, A. J. Ptak, and T. H. Myers, Appl. Phys. Lett. **77**, 2479 (2000).
[23] A. Bell, R. Liu, F. A. Ponce, H. Amano, I. Akasaki, and D. Cherns, Appl. Phys. Lett. **82**, 349 (2003).
[24] G. Namkoong, W. A. Doolittle, and A. S. Brown, Appl. Phys. Lett. **77**, 4386 (2000).
[25] Q. Sun, A. Selloni, T. H. Myers, and W. A. Doolittle, Phys. Rev. B **73**, 155337 (2006).
[26] M. Zhang, P. Bhattacharya, W. Guo, and A. Banerjee, Appl. Phys. Lett. **96**, 132103 (2010).
[27] T. S. Cheng, S. V. Novikov, C. T. Foxon, and J. W. Orton, Solid State Commun. **109**, 439 (1999).
[28] B. Heying, R. Averbeck, L. F. Chen, E. Haus, H. Riechert, and J. S. Speck, J. Appl. Phys. **88**, 1855 (2000).
[29] G. Namkoong, E. Trybus, K. K. Lee, M. Moseley, W. A. Doolittle, and D. C. Look, Appl. Phys. Lett. **93**, 172112 (2008).
[30] B. Gunning, J. Lowder, M. Moseley, and W. A. Doolittle, Appl. Phys. Lett. **101**, 082106 (2012).
[31] J. Neugebauer and C. G. Van de Walle, Proc. Mater. Res. Soc. Symp. **395**, 645 (1996).
[32] B. P. Gunning, C. A. M. Fabien, J. J. Merola, E. A. Clinton, W. A. Doolittle, S. Wang, A. M. Fischer, and F. A. Ponce, J. Appl. Phys. **117**, 045710 (2015).
[33] P. Van Halen and D. L. Pulfrey, J. Appl. Phys. **57**, 5271 (2015).
[34] A. Bhattacharyya, W. Li, J. Cabalu, T. D. Moustakas, D. J. Smith, and R. L. Hervig, Appl. Phys. Lett. **85**, 4956 (2004).
[35] T. A. G. Eberlein, R. Jones, S. Öberg, and P. R. Briddon, Appl. Phys. Lett. **91**, 132105 (2007).
[36] P. Yu and M. Cardona, Fundamentals of Semiconductors: Physics and Materials Properties, 4th edn. (Springer-Verlag, Berlin, Heidelberg, 2010), p. 356.
[37] A. M. Fischer, S. Srinivasan, F. A. Ponce, B. Monemar, F. Bertram, and J. Christen, Appl. Phys. Lett. **93**, 151901 (2008).